Computers in Biology and Medicine 77 (2016) 40–48

Contents lists available at ScienceDirect

Computers in Biology and Medicine

journal homepage: www.elsevier.com/locate/cbm

# Effects of nasal drug delivery device and its orientation on sprayed particle deposition in a realistic human nasal cavity

Xuwen Tong, Jingliang Dong, Yidan Shang, Kiao Inthavong, Jiyuan Tu *

*School of Engineering, RMIT University, PO Box 71, Bundoora, VIC 3083, Australia*

ARTICLE INFO

*Article history:*
Received 12 May 2016
Received in revised form
1 August 2016
Accepted 1 August 2016

*Keywords:*
Nasal spray
Atomization
Deposition fraction
Medications delivery

ABSTRACT

In this study, the effects of nasal drug delivery device and the spray nozzle orientation on sprayed droplets deposition in a realistic human nasal cavity were numerically studied. Prior to performing the numerical investigation, an in-house designed automated actuation system representing mean adults actuation force was developed to produce realistic spray plume. Then, the spray plume development was filmed by high speed photography system, and spray characteristics such as spray cone angle, break-up length, and average droplet velocity were obtained through off-line image analysis. Continuing studies utilizing those experimental data as boundary conditions were applied in the following numerical spray simulations using a commercially available nasal spray device, which was inserted into a realistic adult nasal passage with external facial features. Through varying the particle releasing direction, the deposition fractions of selected particle sizes on the main nasal passage for targeted drug delivery were compared. The results demonstrated that the middle spray direction showed superior spray efficiency compared with upper or lower directions, and the 10 μm agents were the most suitable particle size as the majority of sprayed agents can be delivered to the targeted area, the main passage. This study elaborates a comprehensive approach to better understand nasal spray mechanism and evaluate its performance for existing nasal delivery practices. Results of this study can assist the pharmaceutical industry to improve the current design of nasal drug delivery device and ultimately benefit more patients through optimized medications delivery.



## 1. Introduction

The nasal route for therapeutic agent delivery is an attractive proposition due to the possibility of obtaining a systemic and local response, especially when rapid absorption and effect are desired [5,33]. Nasal sprays are seen as a more efficient way compared with injection or pills to transport drugs with potential use in bypassing the blood-brain barrier [2]. Due to the filtration effect of anterior nostril, majority of sprayed droplets deposits in the anterior nasal cavity [1,14,21,31]. A number of nasal spray studies have reported the low targeted area deposition rate using conventional nasal spray devices. For example, the deposition fraction in the olfactory region only accounts 0.5% of the total delivered therapeutic agents when the particle size is in submicron range [28,34], and this value even becomes negligible for inertial particles [29]. Therefore, comprehensive understanding of nasal spray characteristics and its interaction with the human nasal cavity play essential roles in the design of nasal spray devices and their performance assessment when need.

The nasal cavity is a convoluted anatomy with its primary function to humidify and filter foreign aerosols from the inhaled air before it reaches the lungs (Fig. 1). The main nasal passage may serve as an efficient absorption surface for topically applied therapeutic agents due to the rich vascularization and large surface area proportion [5]. In particular, the olfactory region located at the uppermost of the nasal cavity is the only site in human body where the central nervous system (CNS) is in direct contact with the environment. Intranasally administered drugs once deposited in the olfactory region can migrate across the olfactory mucosa and reach the CNS within minutes, resulting in quick therapeutic onset [10]. However, the nasal anatomy exhibits narrow passageways highlighted by the anterior nasal valve, which limits the transport of sprayed droplets during intranasal spray. This triangular valve-like region has the smallest cross-sectional area located approximately 2–3 cm posterior from the nostril inlet [4] and acts as a flow limiting region [5] before expanding into the main nasal passage. Large aerosols that are unable to navigate through this narrow section can be captured easily. Therefore, the nasal valve presents a major obstacle for effective drug delivery into the main nasal passage where rapid absorption across the mucosa into the blood stream can occur.

* Corresponding author.
*E-mail address:* jiyuan.tu@rmit.edu.au (J. Tu).

http://dx.doi.org/10.1016/j.compbiomed.2016.08.002
0010-4825/

## List of Figures

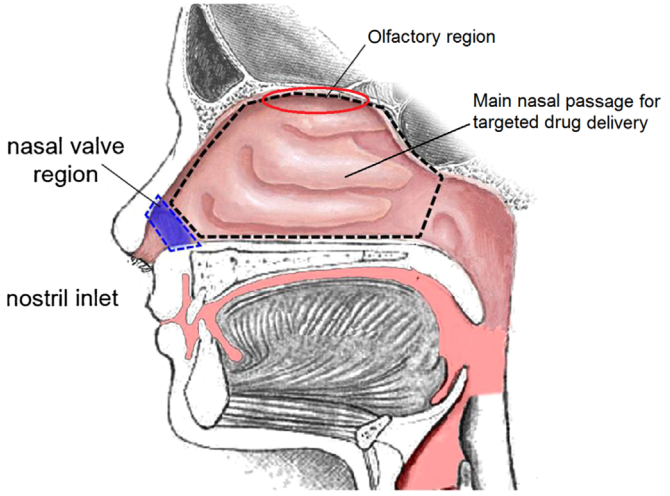


**Fig. 1.** Schematic diagram of nasal cavity showing region for targeted drug delivery for absorption through the mucosa and into the blood stream, where the most obstructive region nasal valve is highlighted by blue. (For interpretation of the references to colour in this figure legend, the reader is referred to the web version of this article.)

Various nasal spray studies adopting human nasal cavity have found the main influences on spray particle deposition involve the nasal cavity geometry and spray parameters (such as droplet size, injected velocity) controlled by the design of nasal spray devices. The aqueous spray pump is the dominant delivery device in the nasal drug delivery market [22] which relies on an actuation force to atomize the drug formulation as it is discharged from the device. The underlying objective of the device is to deliver sufficient drug formulation to the target site.

Cheng et al. [3] evaluated four nasal spray pumps and found that spray plume angle and droplet size distribution were important factors in deposition. Foo et al. [7] found that insertion angle and plume angle are critical factors in determining deposition efficiency and this was confirmed by a number of computational simulations [15,21,8,9]. Kundoor and Dalby [23] evaluated the effect of formulation and administration related variables and found that the deposition area decreased with increasing viscosity but this was mediated by an increase in droplet size and a narrowing of the spray plume. Frank et al. [8,9] investigated effects of the deviated nasal septum on the distribution of spray particles and demonstrated that septal deviation significantly diminished drug delivery on the obstructed side. Our previous study numerically demonstrated the most important parameter was the particle's Stokes number which affects all other parameters on the deposition efficiency [15].

Based on these studies if a spray device can produce a combination of desirable spray characteristics (e.g. spray plume, viscosity, insertion angle, droplet size distribution) then more efficient drug delivery systems can be produced. Despite numbers of relevant studies have been conducted, majority of them were based on experimental measurements or numerical simulation exclusively, and the airflow obstruction effect due to the insertion of nasal spray devices into vestibule region was rarely considered. Although our latest study [14] numerically modelled this airway blockage at one of the nostrils during nasal spray administration, the nasal spray device was over simplified, and its insertion direction and depth was not well aligned with the nasal vestibule.

In the present study, a more realistic nasal spray administration assessment through a combined experimental and numerical approach was presented. Firstly, the initial particle conditions such as spray plume angle, break up length, particle velocity were acquired from Particle Droplet Image Analyser (PDIA). Then, numerical simulations considered the insertion of nasal spray bottle nozzle and human facial effects were conducted. To optimize the drug delivery performance, a spray nozzle orientation adjustment plane was proposed for spray nozzle-nasal valve alignment.

## 2. Methods

### 2.1. Experimental apparatus

The experimental setup for this study is shown in Fig. 2. The main components used in the present study were similar with our previous studies [14,16], which mainly includes the automated actuation system and the visualization system. In our previous studies, the pneumatic actuator was driven by constant pressure through pressure regulator to achieve a relatively steady spray plume, while this driven force failed to represent the human actuation behaviour. In the present study, a programmable logic control (PLC) unit (model: 1760-L12BWB; Allen Bradley, Lumberton, New Jersey) was employed to control the two-way solenoid valve which drives speed controllers for spray device actuation. Thus, the strength of actuation force is controllable during the flow visualization. To represent adult's actuation behaviour, 20 adult volunteers were invited to press the spray bottle with strain gauge sensors attached. In this study, a small strain gauge in rectangular shape was attached to the nasal spray bottle wall. During spray, the nasal spray device is compressed by the applied force, and a slight vertical deformation (compression) occurs. Meanwhile, the firmly attached strain gauge sensor will capture the ratio of compression length to its original chip length and send this information to the recorder in terms of electronic signal. Therefore, the spray bottle deformation characteristics during actuation can be recorded for each person invited. This actuation action was repeated 5 times for each volunteer, and the averaged microstrain profile was presented in Fig. 3. Through adjusting the programmable PLC regulator and input pressure, a programmed realistic actuation strain profile was achieved with reasonably good accuracy.

For capturing of the spray, an Oxford laser PDIA system was used. The CCD camera was mounted on a traversing unit which allowed precise movements in all three coordinates to capture the spray plume in full. A long distance microscope lens providing a magnification of 2.46 was used. This enables to capture a physical region of 192 mm $\times$ 120 mm with a resolution of 1280 $\times$ 800 for each image. To ensure the camera view can be fulfilled with even bright illumination, a 2000 W spotlight was mounted in line with the camera lens.

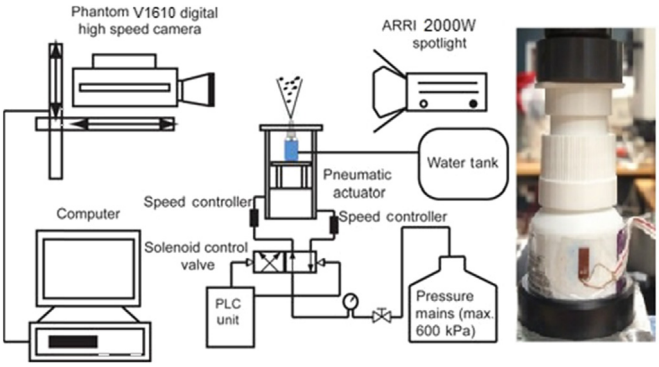


**Fig. 2.** A schematic of the experimental setup showing the automated actuation system and the visualization system.

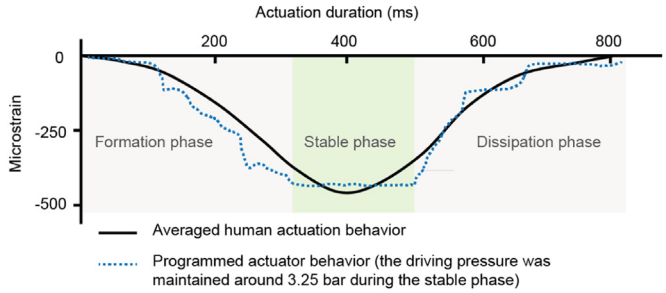


**Fig. 3.** Monitored microstrain profile generated by the programmable nasal spray actuator to match averaged adult's actuation behaviour.

### 2.2. Numerical setup

Nasal cavity geometry was obtained through a CT scan of a healthy 25-year-old, Asian male (170 cm height, 75 kg mass). Model reconstruction procedure has been detailed in our previous study [17], but facial features were also included in the present model to better capture the airflow patterns within breathing zone (especially near the nostril inlets). Maximum insertion depth $L_d$ of 11 mm was applied for the spray nozzle when considering the presence of driving fingers (Fig. 4).

Fig. 5 details the anatomical features of the vestibule region in terms of cross-sectional planes. It was found that the vestibule passage continuously narrows from the nostril to the nasal valve, and the nasal valve applies the main restriction for the spray plume development due to its mostly narrowed width (2.4 mm). Due to this limited width at the vicinity of nasal valve, a poor spray nozzle - nasal valve alignment will filter majority of the sprayed droplets and significantly lower the drug delivery performance.

To optimize the spray nozzle - nasal valve alignment, a spray nozzle adjustment plane was proposed in Fig. 6. The spray nozzle was aimed at the centre line of the nasal valve (Fig. 6a), and its orientation is adjustable within the nozzle orientation adjustment plane (Fig. 6b). Angle $\alpha$ and $\beta$ indicates the upwards and downwards angle adjustment allowance, respectively. For the purpose of simplification, three representative spray orientations, the centre direction (OA), the tilted up direction (OB, halfway of the upwards adjustment allowance), and the tilted down direction (OC, halfway of the downwards adjustment allowance), were considered to compare their effects on the sprayed particle deposition performance.

As detailed in our previous studies [15,16], similar mesh generation and independence test have been applied to the present CAD model, the optimum mesh sizes are 1,921,484 cells. The

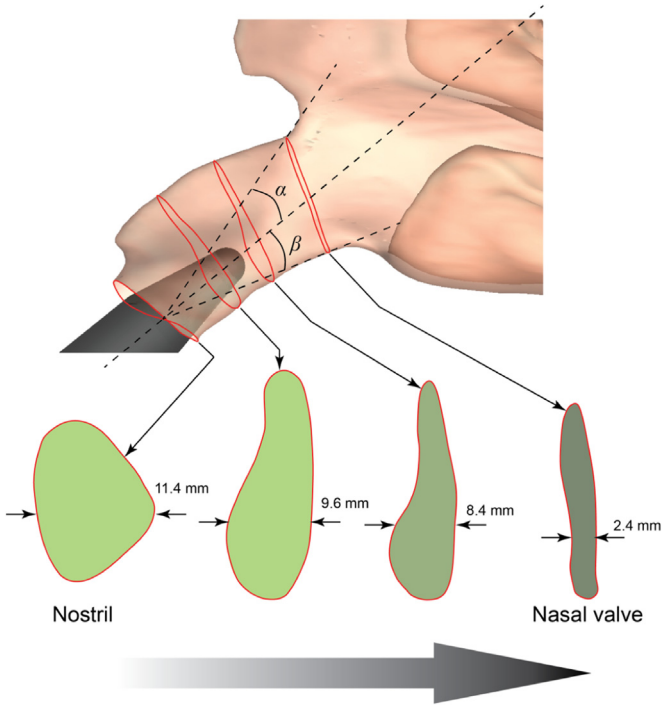


**Fig. 5.** The space variation of vestibule passage for the nasal spray plume development. The cross-sectional area of nasal vestibule passage is significantly narrowed from a circle to a strip shape, which greatly limits the space for nasal spray delivery.

computational mesh results are shown in Fig. 7 with a coronal plane and the outlet of the computational domain showing the internal mesh with a mesh refined region near the walls.

ANSYS-Fluent v14.5 was used to predict the flow field of the continuum gas phase under steady-state conditions by solving the full Navier–Stokes equations. The QUICK scheme was used to approximate the momentum equation while the pressure-velocity coupling was realized through the SIMPLE method. In the present study, only one flow rate 15 L/min was considered, which represents a rest breathing condition for adults. Since the nostril on the side not receiving the medication (the right nostril in the present study) is recommended to be closed by a finger according to instructions of some commercial nasal spray devices, the right nostril was closed in this study. Naftali et al. [25] and Schroeter et al. [27] have suggested that a laminar flow regime dominates the nasal main passage for flow rates around 15 L/min. However,

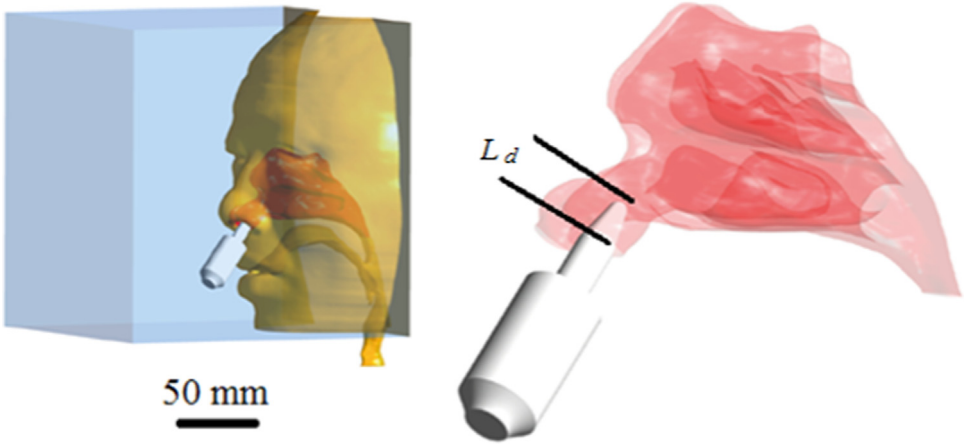


**Fig. 4.** Computational model including facial features and nasal spray device. The insertion depth $L_d$ for the nasal device nozzle is 11 mm considering the presence of driving figures.

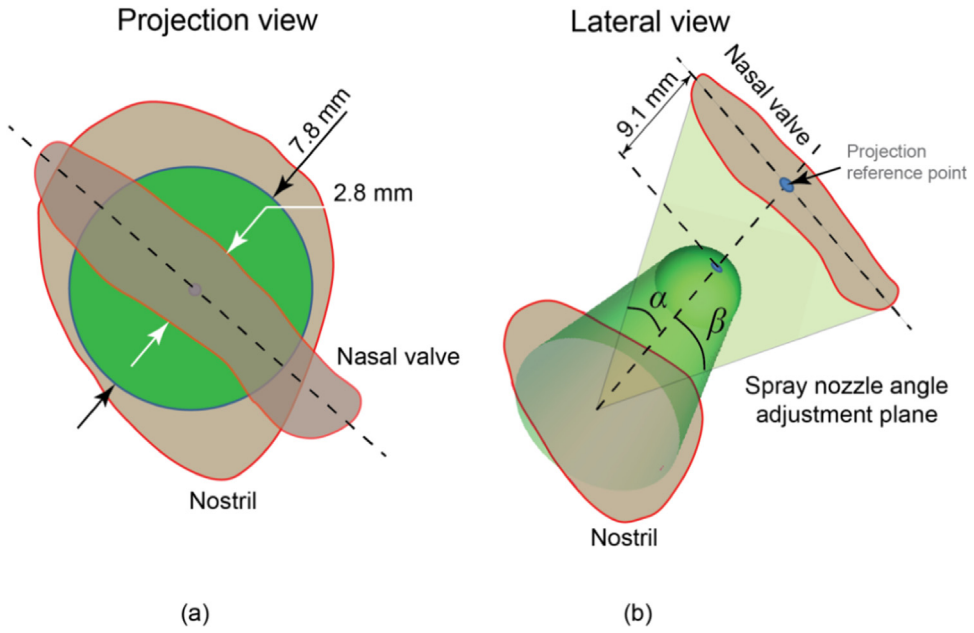


**Fig. 6.** The alignment of the spray nozzle and the nasal valve. The proposed alignment suggests the nozzle tip aims to the centre line of the nasal valve plane, and $\alpha$, $\beta$ stands for the upwards and downwards orientation adjustment angle allowance.

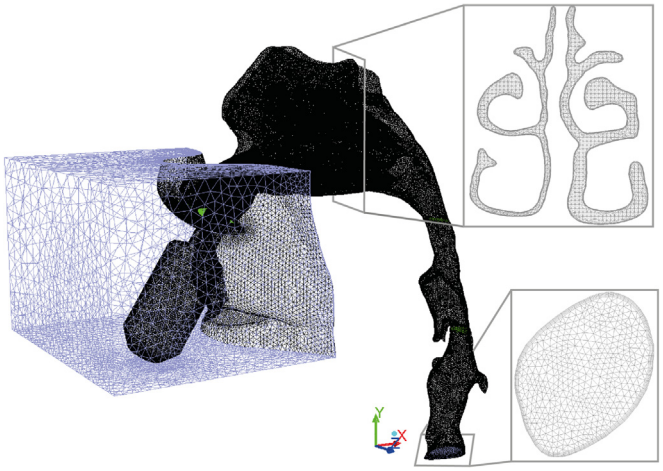

**Fig. 7.** Computational mesh results including the presence of a nasal spray device. Prism layers were imposed at the near wall region to better represent the airflow and particle deposition patterns.

with the closure of the right nostril and the insertion of spray nozzle, significant velocity acceleration and turbulent flow are expected at the anterior vestibule region of the left nasal cavity. Therefore, transitional SST model was used for flow filed simulation for the right nostril closed mode.

Our previous study [12] revealed majority of the sprayed particle size ranges between 50 μm and 110 μm, and fine micron particles (diameter smaller than 20 μm) only account a very small volume fraction (less than 2%) in the whole size spectrum using the current commercial nasal spray devices. Despite the volume percentage for fine micron particles remains relatively low, their unique particle deposition characteristics may serve the drug delivery purpose better than large particles. Therefore, in the present study, four typical particle sizes, 5, 10 15, 50 μm were selected to detail their deposition characteristics. For each simulation, 10,000 particles were released at the spray break-up plane [19], and the particle initial velocity was set as 15 m/s according to our previous measurement.

## 3. Results

### 3.1. Spray plume outline detection

The spray plume outline was detected by Sobel method, which was developed by Sobel [30]. It is a derivative based edge detection algorithm which is able to calculate the boundary of the spray cone by implements convolution with Sobel kernels. The subject edge was determined by determining the greatest gradient of change of the intensity of pixels. It gives the direction of the change of colour and the change rate in that direction. The Sobel method was applied through MATLAB coding on captured 200 images recorded during the fully developed stage for plume outline detection. To minimize the computational time, a $600 \times 300$ pixel field of view (white rectangular box in Fig. 8a) was selected to cover a 90 mm × 45 mm view size. After extracting outlines for all images, they were stacked together and an overlapped view is shown in Fig. 8b, in which the outlines show a minimal deviation at the near-nozzle region while obvious oscillating can be observed further downstream of the spray plume. Despite the spray outline deviation exists among all sampled images, the images extracted during the fully developed stage maintained a relatively stable outline formation, which can provide statistically accurate spray cone angle information.

### 3.2. Near-nozzle spray characteristics

Due to the instability caused by the shearing interaction with the surrounding air, the liquid sheet near the spray nozzle disintegrates into ligaments, and the distance at which this occurs from the spray nozzle is referred as the breakup length ($L$). Because of the oscillating nature of the liquid sheet, it is very difficult to utilize the edge detection scheme for the determination of breakup length. Therefore, in the current study, visual inspection was performed over 200 images extracted during the fully developed stage, which is proven to be statistically sufficient to get an averaged value. For the current nasal spray device, its spray orifice radius $r_o$ is 0.35 mm, the breakup length $l$ indicating the distance between the orifice and the downstream location at which clearly formed particles were observed is 2.5 mm, and the

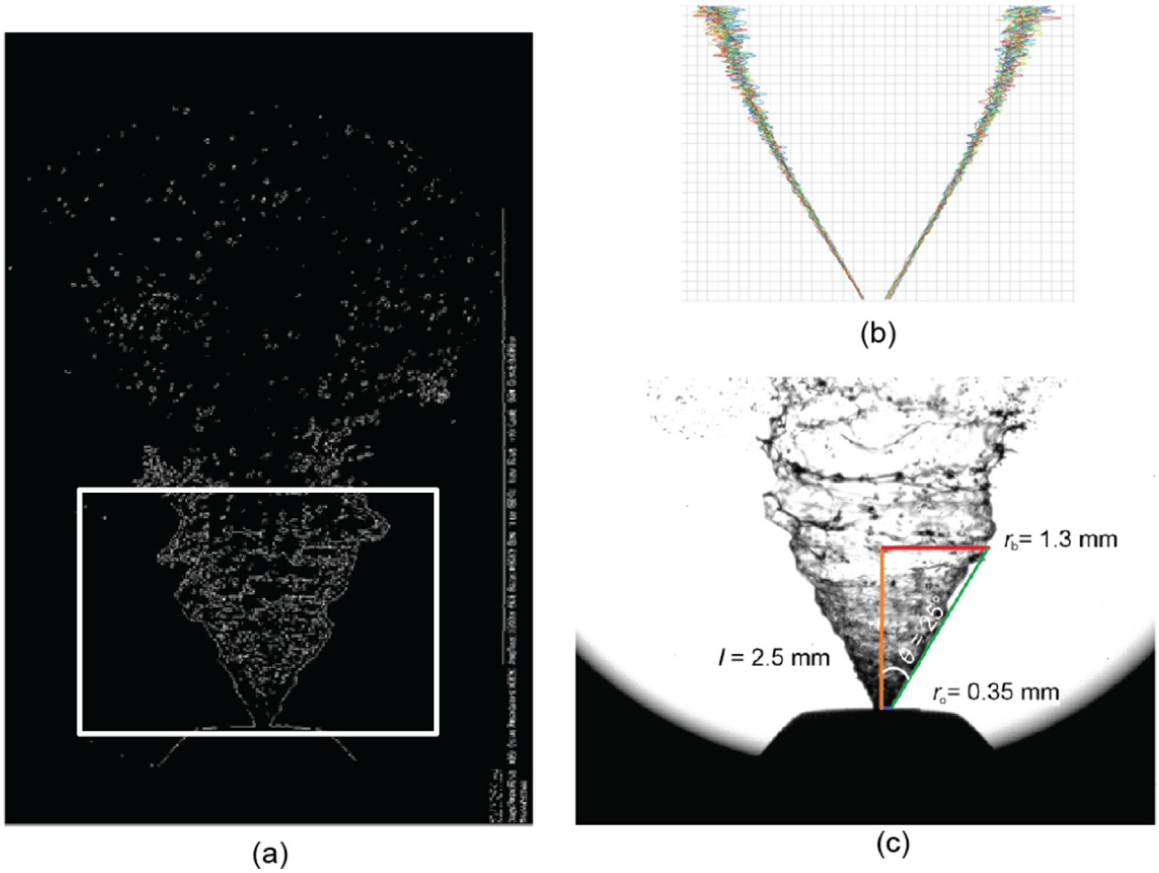


**Fig. 8.** Detection of spray plume outline, and external nasal spray characteristics indicating the break-up length $l$ break-up radius $r$ and half spray angle $\Theta$. In this study, the tested nasal spray device gives a break-up length of 2.5 mm, break-up radius of 1.3 mm, and a spray angle of 50°.

spray diameter is 2.6 mm ($r_b$=1.3 mm). Consequently, the formed spray angle $2\Theta$ is 50° (Fig. 8c). All these information were input into following CFD models for the introduction of particles into the computational domain.

### 3.3. Computational model validation

In particle deposition studies, the inertial parameter, $I$, is a widely adopted parameter that compares deposition against different flow rates and particle sizes at aerodynamic diameters. It is given by

$$I = Qd_{ae}^2$$

where $Q$ is the airflow rate, $d_{ae}$ is the aerodynamic diameter given in μm.

To validate the numerical modelling approach accuracy, monodispersed particles in the range of 1–30 μm were released passively into the nasal cavity with flow rates of 5, 7.5, 10 and 15 L/min. The particle deposition as a function of the inertial parameter is shown in Fig. 9. The numerical simulation results were compared with other relevant experimental [3,20] and numerical data [26,29], and a similar deposition trend pattern was found. Differences in deposition may be attributed to the inter-subject variability between the current nasal model (25-year-old Asian male) with the nasal cavity model obtained by Kelly et al. [20] (53-year Caucasian male). Haussermann et al. [11] also demonstrated that nasal cavity replicas with wider airways can cause less deposition due to secondary flow. Furthermore, the comparison differences can also be explained by the particle relaxation time, $\tau_p$, which represents a typical timescale of the particle's reaction to changes in the carrier airflow. It is given by

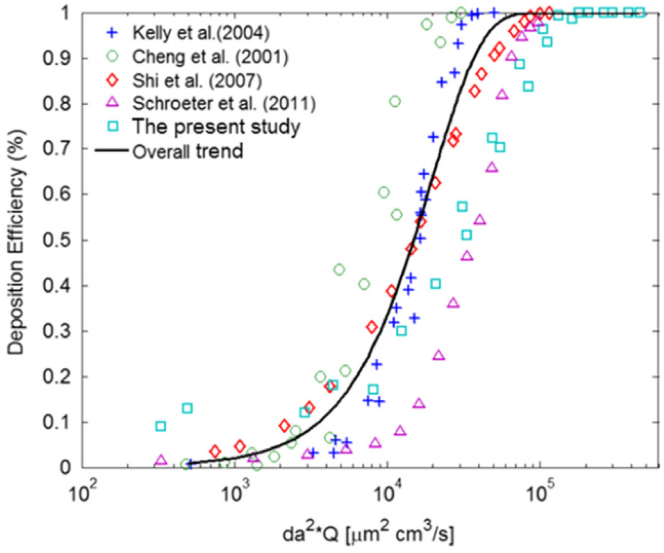


**Fig. 9.** Numerical simulation results for total deposition of particles against inertial parameter compared with other experimental and numerical data.

$$\tau_p = \frac{\rho_p d_{ae}^2}{18\mu}$$

here $\rho_p$ is the particle density, $\mu$ is the dynamic viscosity of the carrier airflow.

For $I$ less than 2000 μm² cm³/s, particles have a short relaxation time (a typical timescale of the particle's reaction to changes in the carrier airflow), which allows the particles to adjust to flow

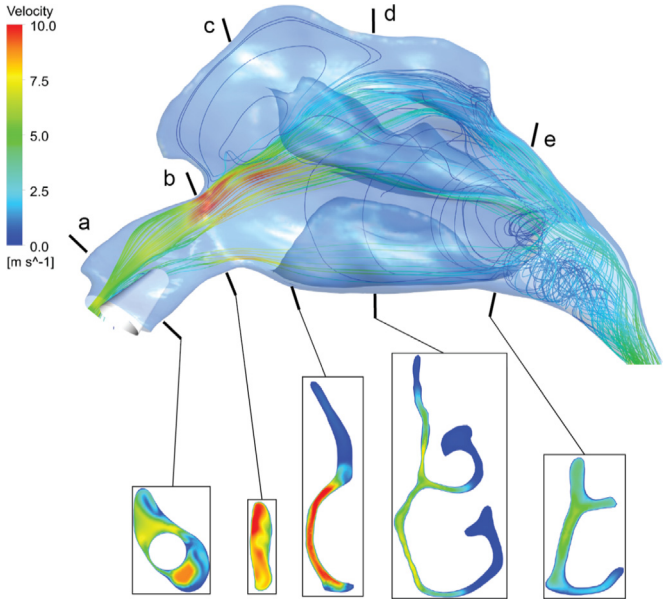


**Fig. 10.** Nasal cavity streamlines in the drug administering half cavity with the other nostril closed.

streamlines more easily. Hence the inter-subject geometrical variability is less significant, and the comparison between the CFD simulation and the experimental data is fairly similar. As the inertial parameter *I* increases, the particles relaxation time increases. The particles are more likely to continue a liner trajectory rather than following highly curved streamlines. The differences in geometries that cause curvatures in streamlines are therefore significant for larger inertial particles.

### 3.4. Airflow field

The main flow features within the drug administering half cavity nasal cavity (left chamber) is depicted in Fig. 10. Flow acceleration, separation and vertical flow are three main features. The acceleration found at the vicinity of the nasal valve is mainly due to the reduced cross-sectional area, flow separation found at the superior main passage is mainly due to the sudden vertical passage expansion, while the vertical flow observed at the posterior of the nasal cavity is attributed to the guiding effect of middle and inferior turbinates. Despite a rest inhalation flow condition 15 L/min was adopted in this study, significant airflow accelerations were found at the vestibule and the anterior of the main passage with airflow velocity peaking at 11.7 m/s at the nasal valve (Plane b). In comparison, the streamlines for a plain nasal cavity model were provided in our previous study [14], and maximum velocity was around 5 m/s at the vicinity of the nasal valve. This is attributed to the closure of the right nostril as recommended by the user instructions from the nasal spray provider, and the resultant airflow rate in the right cavity was doubled than previous case.

The presence of the spray device is highlighted in 'Plane a', the effective area of the right nostril to the open air was significantly reduced with apparent airflow acceleration. Different from our previous study [14], since a more realistic nasal spray head was created in study, flow separation was not observed in its peripheral confined space. In addition, due to the closure of the left nostril, the airflow speed at the spray head periphery was doubled from less than 3.5 m/s to 7.5 m/s.

### 3.5. Particle deposition comparison

Depositions of selected micron particles were compared in Fig. 11. To isolate the particle size effect, all other conditions such as the spray direction, spray plume external characteristics, initial velocity were kept identical. The left half nasal chamber was divided into three main regions: the vestibule (***I***), the main passage (***II***), and the pharynx (***III***) based on the anatomical features and epithelium types for drug delivery performance assessment. It is well known that the main passage offers a large mucosal surface with richly vascularized for drug absorption [18,24]. Therefore, in this study the main passage was selected as the targeted area for drug delivery performance assessment. Furthermore, to distinguish the deposition along the septum or the outer lateral wall of the main passage, the deposited particles were coloured into red or green, respectively.

For the 5 μm case (Fig. 11a), only 9.6% of sprayed particles were deposited in the main passage, and most of them were captured by the nasal septum (in red colour). Very few amount (0.4%) of particles was deposited in the pharynx region, indicating large proportion of sprayed particles (90.1%) was carried by the airflow and travelled further downstream of the respiratory system. For the

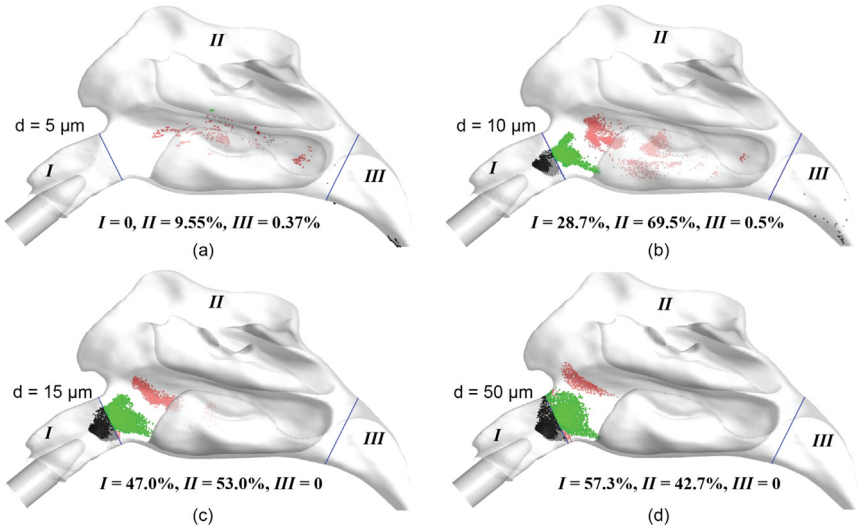


**Fig. 11.** Sprayed particle deposition comparison among four selected micron sizes. Particles deposited on the vestibule region is coloured in black, that deposited on the outer lateral wall of the cavity is coloured in green, while that deposited on the inner septal wall is coloured in red. (For interpretation of the references to colour in this figure legend, the reader is referred to the web version of this article.)

10 μm particles (Fig. 11b), the particle deposition percentage significantly increased with a 98.7% total deposition in the whole chamber. In detail, 28.7% of particles were deposited at the vestibule region shortly after released from the spray orifice, and 69.5% of particles were captured by the inferior main passage with a 25.2% for the lateral wall and 44.30% for the nasal septum. The deposition at the nasal septum showed a widely dispersed pattern along the inferior chamber, while the particle distribution at the lateral wall was highly condensed at the anterior. For 15 μm and 50 μm cases (Fig. 11c and d), both of them showed a total deposition in the nasal chamber with similar patterns. More early deposition was found at the vestibule region (47.0% for the 15 μm case, and 57.3% for the 50 μm case), leaving less particles trapped at the anterior of the lower passage.

Besides with the particle size, another key factor, the influence of spray directions was considered. To quantify drug delivery performance in the left half nasal cavity, particle deposition intensity along the nasal septum and lateral wall was provided in Fig. 12. Deposition intensity indicates the accumulated deposition fraction on each cross-sectional slice over the total nasal deposition, $n_{slice}/n_{cavity}$[6]. Therefore, the particle penetration depth along with its corresponding intensity can be quantified for different spray orientations.

In general, the maximum particle penetration depth was found at somewhere along the nasal septum (red solid line) for all studied particle sizes and spray directions, and peak deposition intensity along the lateral wall all occurred right after the nasal valve, indicating a direct impact for all sprayed particles along this side. That is mainly due to the highly bended lateral wall at the vicinity of the nasal valve, which captures almost all sprayed particles along this side. While for the septum side, the relatively unchanged wall boundary allows introduced particles can travel further downstream of the nasal cavity. In detail, for spray direction OA, the maximum particle penetration depth (4.5 cm) was found at the septum wall for the 10 μm with a deposition intensity of 0.2. With the increase of the particle size, the penetration depth was reduced towards the nasal valve due to the increased particle inertia. For spray direction OB, similar penetration pattern was found, which is the 10 μm particles deposited with the largest penetration depth (3.2 cm) with intensity of 0.8 along the nasal septum, while the penetration intensity along the lateral wall side peaked at 1.1. For spray direction OC, the deposition pattern significantly changed. The particle penetration intensity along the septum wall was greatly reduced to less than 0.2. While for the lateral side, the penetration depth was slightly increased for all particle sizes, indicating more particles can travel further downstream along the later wall side when lower the nasal spray direction.

## 4. Discussion and conclusions

This study provides a systematically nasal spray performance evaluation on the basis of high speed imaging for spray outline analysis, medical imaging (CT scan in this study) and CFD simulation. Influence factors such as breathing condition, spray direction (spray nozzle - nasal valve alignment), and medication droplets size were considered.

Despite the nasal sprays provide non-invasive quick therapeutic onset and have been widely applied for the treatment of cold and allergy, poorly designed spray nozzle or incorrect use of spray devices will significantly affect the treatment outcome. *In vitro* spray characterization tests conducted by Suman et al. [32] investigated the effects of influential factors including mean volume diameters, spray angle, spray width observed from two spray pumps on the spray performance. Their results suggest that current measures of in vitro performance, particularly spray angle and spray pattern, may not be clinically relevant due to the absence of nasal anatomy, human actuation behaviour, and other operational factors. Given the confines of the nasal passage, it is extremely unlikely that an emitted plume would be able to freely develop in the nose in the same manner it does when fired into an unobstructed space.

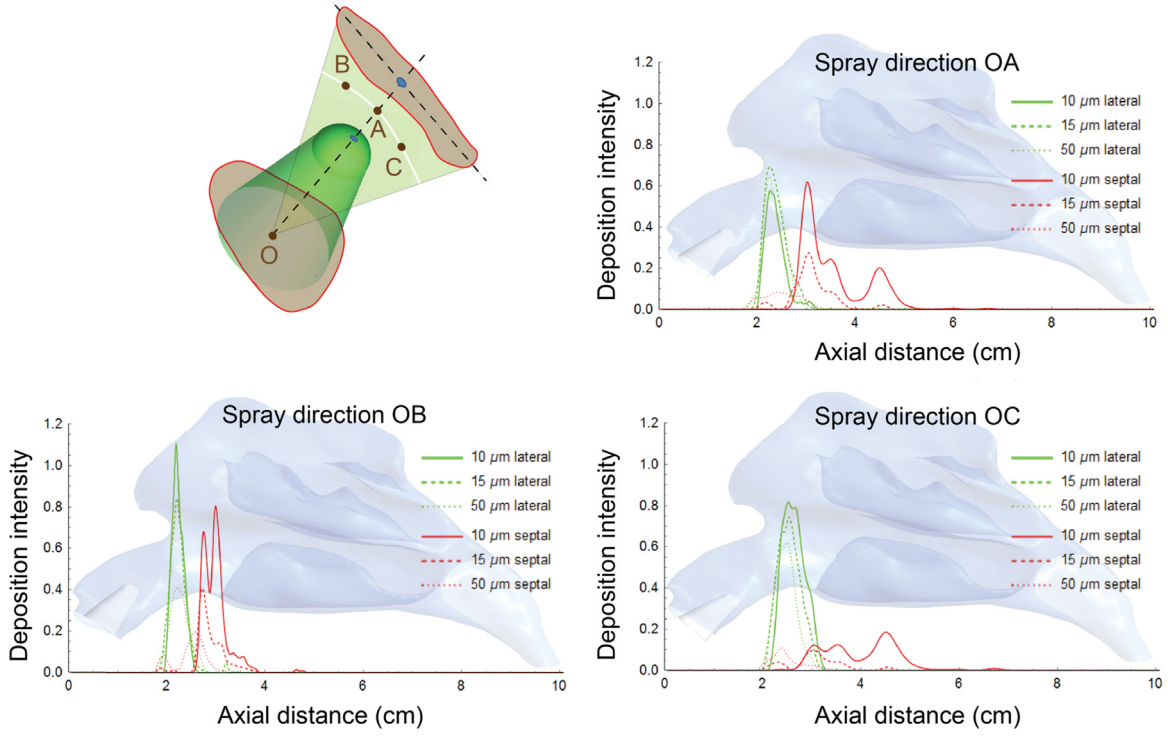


**Fig. 12.** Deposition intensity comparison among different spray directions. Particles deposited on the outer lateral wall of the cavity is coloured in green, while that deposited on the inner septal wall is coloured in red. (For interpretation of the references to colour in this figure legend, the reader is referred to the web version of this article.)

It is well known that the anterior portions of the nose are lined with non-ciliated squamous epithelium, which is not suitable for drug absorption [5]. As one passes deeper into the nasal cavity, the mucosal surface gradually changes to ciliated respiratory epithelium, where branches of the ophthalmic and maxillary arteries enable the rapid absorption of drugs across the mucosa and into the bloodstream. Therefore, the nasal spray efficiency is largely limited as majority of the medication agents are blocked at the anterior nose. However, particular nasal spray direction well aligned with the nasal valve can improve the particle deposition fraction in the targeted nasal area. In the present study, the middle spray direction OA showed superior spray efficiency compared with upper or lower directions. It should be noted that the optimal spray direction may vary between different matches of nasal spray devices and nasal cavities, as the interaction between the nasal spray and human nasal cavity dominates the drug delivery process.

Lastly, for all examined micron-sized agents, the 10 μm agents were the most suitable particle size as majority of sprayed agents can be delivered to the targeted area, the main passage. This is mainly attributed to the preferred particle relaxation time, preventing the medication agents in this size from direct impaction at the vicinity of nasal vestibule region and maximizing the deposition in the main passage. While for relative smaller agents (e.g. 5 μm), the airflow dominates particle motion due to the smaller particle relaxation time scale, and majority of sprayed agents are conveyed to deeper respiratory tract, which is not desired. For large sized particles such as 15 μm or 50 μm agents, their motion is dominated by the inertia, which results a direct impaction in anterior nose (the nasal vestibule) immediately after the nasal spray.

In the present study, only particle deposition characteristics of selective particle sizes were discussed, while additional efforts are still needed for the interpretation of the realistic nasal spray performance. Our previous study [13] has investigated the spray size distribution under different actuation pressure, and the results showed that higher actuation pressure produces smaller droplets in the atomization. Additionally, stronger typical adult users' actuation pressure can produce a longer period of the fully developed spray stage, and the droplet size delivered during the stable phase is associated with finer droplets than during the formation and dissipation phases. Despite different actuation pressure varies from 2.05 bar to 2.65 bar were applied, the volume fraction of particles smaller than 50 μm was less than 5% compared with the volume fractions of other particle sizes within the whole recorded particle size spectrum ranges from 0 to 400 μm [13]. Therefore, although particle deposition fractions of selective particle sizes were reported in the presented study, additional interpretation efforts are needed in the overall performance assessment of nasal spray devices. Other limitations of this study include the assumption of steady flow, selective release positions, the rigid airway wall assumption and the use of only one nasal cavity also influence the realism of the numerical predictions. These limitations remain to be included in future studies.

## Acknowledgements and disclosures

This work was supported by the Australian Research Council (Project ID: DP160101953), and the authors report no conflicts of interest in this work.

## References

[1] M. Bergstrom, L.M.R. Cass, S. Valind, G. Westerberg, E.L. Lundberg, S. Gray, A. Bye, B. Langstrom, Deposition and disposition of [C-11]zanamivir following administration as an intranasal spray - evaluation with positron emission tomography, Clin. Pharmacokinet. 36 (1999) 33–39.
[2] B.E. Bleske, E.W. Warren, T.L. Rice, M.J. Shea, G. Amidon, P. Knight, Comparison of intravenous and intranasal administration of epinephrine during CPR in a canine model, Ann. Emerg. Med. 21 (9) (1992) 1125–1130.
[3] Y.S. Cheng, T.D. Holmes, J. Gao, R.A. Guilmette, S. Li, Y. Surakitbanharn, C. Rowlings, Characterization of nasal spray pumps and deposition pattern in a replica of the human nasal airway, J. Aerosol Med.: Depos. Clear. Eff. Lung 14 (2) (2001) 267–280.
[4] P. Cole, The four components of the nasal valve, Am. J. Rhinol. 17 (2) (2003) 107–110.
[5] P.G. Djupesland, Nasal drug delivery devices: characteristics and performance in a clinical perspective – a review, Drug Deliv. Transl. Res. 3 (1) (2013) 42–62.
[6] J.L. Dong, Y.D. Shang, K. Inthavong, J.Y. Tu, R. Chen, R. Bai, D. Wang, C. Chen, Comparative numerical modeling of inhaled nanoparticle deposition in human and rat nasal cavities, Toxicol. Sci. 152 (2) (2016) 284–296.
[7] M.Y. Foo, Y.S. Cheng, W.C. Su, M.D. Donovan, The influence of spray properties on intranasal deposition, J. Aerosol Med.-Depos. Clear. Eff. Lung 20 (4) (2007) 495–508.
[8] D.O. Frank, J.S. Kimbell, D. Cannon, S.S. Pawar, J.S. Rhee, Deviated nasal septum hinders intranasal sprays: a computer simulation study, Rhinology 50 (3) (2012) 311–318.
[9] D.O. Frank, J.S. Kimbell, S. Pawar, J.S. Rhee, Effects of anatomy and particle size on nasal sprays and nebulizers, Otolaryngol.-Head Neck Surg. 146 (2) (2012) 313–319.
[10] L.R. Hanson, W.H. Frey, Strategies for intranasal delivery of therapeutics for the prevention and treatment of neuroAIDS, J. Neuroimmune Pharmacol. 2 (1) (2007) 81–86.
[11] S. Haussermann, A.G. Bailey, M.R. Bailey, G. Etherington, M. Youngman, The influence of breathing patterns on particle deposition in a nasal replicate cast, J. Aerosol Sci. 33 (6) (2002) 923–933.
[12] K. Inthavong, M.C. Fung, X.W. Tong, W. Yang, J.Y. Tu, High resolution visualization and analysis of nasal spray drug delivery, Pharm. Res. 31 (8) (2014) 1930–1937.
[13] K. Inthavong, M.C. Fung, W. Yang, J.Y. Tu, Measurements of droplet size distribution and analysis of nasal spray atomization from different actuation pressure, J. Aerosol Med. Pulm. Drug Deliv. 28 (1) (2015) 59–67.
[14] K. Inthavong, Q.J. Ge, C.M.K. Se, W. Yang, J.Y. Tu, Simulation of sprayed particle deposition in a human nasal cavity including a nasal spray device, J. Aerosol Sci. 42 (2) (2011) 100–113.
[15] K. Inthavong, Z.F. Tian, H.F. Li, J.Y. Tu, W. Yang, C.L. Xue, C.G. Li, A numerical study of spray particle deposition in a human nasal cavity, Aerosol Sci. Technol. 40 (11) (2006), 1034-U1033.
[16] K. Inthavong, Z.F. Tian, J.Y. Tu, W. Yang, C. Xue, Optimising nasal spray parameters for efficient drug delivery using computational fluid dynamics, Comput. Biol. Med. 38 (6) (2008) 713–726.
[17] K. Inthavong, J. Wen, J.Y. Tu, Z.F. Tian, From CT scans to CFD modelling - fluid and heat transfer in a realistic human nasal cavity, Eng. Appl. Comput. Fluid Mech. 3 (3) (2009) 321–335.
[18] N. Jones, The nose and paranasal sinuses physiology and anatomy, Adv. Drug Deliv. Rev. 51 (1–3) (2001) 5–19.
[19] J.A. Keeler, A. Patki, C.R. Woodard, D.O. Frank-Ito, A computational study of nasal spray deposition pattern in four ethnic groups, J. Aerosol Med. Pulm. Drug Deliv. 29 (2) (2016) 153–166.
[20] J.T. Kelly, B. Asgharian, J.S. Kimbell, B.A. Wong, Particle deposition in human nasal airway replicas manufactured by different methods. Part I: inertial regime particles, Aerosol Sci. Technol. 38 (11) (2004) 1063–1071.
[21] J.S. Kimbell, R.A. Segal, B. Asgharian, B.A. Wong, J.D. Schroeter, J.P. Southall, C. J. Dickens, G. Brace, F.J. Miller, Characterization of deposition from nasal spray devices using a computational fluid dynamics model of the human nasal passages, J. Aerosol Med.: Depos. Clear. Eff. Lung 20 (1) (2007) 59–74.
[22] V. Kundoor, R.N. Dalby, Assessment of nasal spray deposition pattern in a silicone human nose model using a color-based method, Pharm. Res. 27 (1) (2010) 30–36.
[23] V. Kundoor, R.N. Dalby, Effect of formulation- and administration-related variables on deposition pattern of nasal spray pumps evaluated using a nasal cast, Pharm. Res. 28 (8) (2011) 1895–1904.
[24] N. Mygind, R. Dahl, Anatomy, physiology and function of the nasal cavities in health and disease, Adv. Drug Deliv. Rev. 29 (1–2) (1998) 3–12.
[25] S. Naftali, M. Rosenfeld, M. Wolf, D. Elad, The air-conditioning capacity of the human nose, Ann. Biomed. Eng. 33 (4) (2005) 545–553.
[26] J.D. Schroeter, G.J.M. Garcia, J.S. Kimbell, Effects of surface smoothness on inertial particle deposition in human nasal models, J. Aerosol Sci. 42 (1) (2011) 52–63.
[27] J.D. Schroeter, J.S. Kimbell, B. Asgharian, Analysis of particle deposition in the turbinate and olfactory regions using a human nasal computational fluid dynamics model, J. Aerosol Med.: Depos. Clear. Eff. Lung 19 (3) (2006) 301–313.
[28] H. Shi, C. Kleinstreuer, Z. Zhang, Laminar airflow and nanoparticle or vapor deposition in a human nasal cavity model, J. Biomech. Eng.: Trans. ASME 128 (5) (2006) 697–706.
[29] H.A. Shi, C. Kleinstreuer, Z. Zhang, Modeling of inertial particle transport and deposition in human nasal cavities with wall roughness, J. Aerosol Sci. 38 (4) (2007) 398–419.
[30] I. Sobel, Neighborhood coding of binary images for fast contour following and general binary array processing, Comput. Graph. Image Process. 8 (1) (1978) 127–135.

[31] J.D. Suman, B.L. Laube, R. Dalby, Comparison of nasal deposition and clearance of aerosol generated by a nebulizer and an aqueous spray pump, Pharm. Res. 16 (10) (1999) 1648–1652.
[32] J.D. Suman, B.L. Laube, R. Dalby, Validity of in vitro tests on aqueous spray pumps as surrogates for nasal deposition, absorption, and biologic response, J. Aerosol Med.: Depos. Clear. Eff. Lung 19 (4) (2006) 510–521.
[33] T.Y. Ting, I. Gonda, E.M. Gipps, Microparticles of polyvinyl-alcohol for nasal delivery 0.1. generation by spray-drying and spray-desolvation, Pharm. Res. 9 (10) (1992) 1330–1335.
[34] J.X. Xi, P.W. Longest, Numerical predictions of submicrometer aerosol deposition in the nasal cavity using a novel drift flux approach, Int. J. Heat Mass Transf. 51 (23–24) (2008) 5562–5577.